7th International Conference on Modelling and Simulation in Nuclear Science and Engineering (7ICMSNSE)
Ottawa Marriott Hotel, Ottawa, Ontario, Canada, October 18-21, 2015

7ICMSNSE-068

Numerical Predictions of Heat Transfer and Pressure Tube/Calandria Tube Deformation During Calandria-Tube Strain Contact Boiling (CSCB) Tests

A. Tanase, J. Szymanski , M. El-Hawary and A. Delja
Canadian Nuclear Safety Commission, Ottawa, Ontario, Canada
aurelian.tanase@cnsc-ccsn.gc.ca

Abstract

The assessment of fuel channel integrity during large break LOCA requires adequate prediction of the thermal-mechanical behaviour of the fuel channel following pressure tube ballooning into contact with the calandria tube. Analytical models developed for this purpose need to be calibrated and validated against experimental data. A new series of contact boiling tests was initiated by CNSC to provide additional data on calandria tube straining behaviour after PT/CT contact. This paper presents selected results of the first of these tests and their comparisons with predictions using analytical methodology developed by CNSC staff.

Keywords: Thermalhydraulics, Fuel and Fuel Channels, moderator subcooling .

1. Introduction

In CANDU reactors, the moderator acts as a heat sink to maintain Fuel Channel Integrity (FCI) in accident scenarios where the pressure tube (PT) balloons into contact with the calandria tube (CT). The moderator temperature should be sufficiently low to act as an effective heat sink. The adequacy of moderator temperature is confirmed by safety analysis. Analytical models developed for this purpose need to be fine-tuned and validated against experimental data.

Fuel channel safety can be characterized by the maximum plastic PT/CT strain during heat-up transients. The CANDU industry has proposed a moderator subcooling requirements model [1] which was developed and validated using data from a large number of contact boiling tests [2]. A limit of 2% hoop strain was selected by the CANDU industry based on experimental evidence including the results of full scale contact boiling experiments. A recent review by Canadian Nuclear Safety Commission (CNSC) staff identified the need for additional contact boiling experiments resulting in calandria tube strain. The objective of the test series (Calandria-tube Strain Contact Boiling –CSCB) is to provide further data that will confirm the acceptance criterion of 2% calandria tube strain for assessing moderator subcooling requirements model and support the correlation adopted for calandria tube rewet temperature.

The paper summarizes the process of development and benchmarking of simulation tool using the experimental results from first two sets of CSCB series (CSCB1 and CSCB2)[3]. The experimental results from the International Atomic Energy Agency (IAEA) International Collaborative Standard Problem (ICSP) test [4] were also included in the analysis.

2. Experiment setup

The CSCB and ICSP tests were performed by Canadian Nuclear Laboratories (CNL) in the Fuel Channel High Temperature Heat Transfer (FCHTHT) laboratory at Chalk River, which has an experimental facility designed to study the behaviour of CANDU fuel channels under postulated accident scenarios. The facility has an electrically heated test section consisting of a segment of fuel channel with a graphite heater inside, submerged in an open tank filled with water that can be heated to a desired temperature. The tank has transparent windows to allow observation and video recording of the boiling on the outside surface of the calandria tube during the test. A lateral view of test section and water tank is presented in Figure 1.

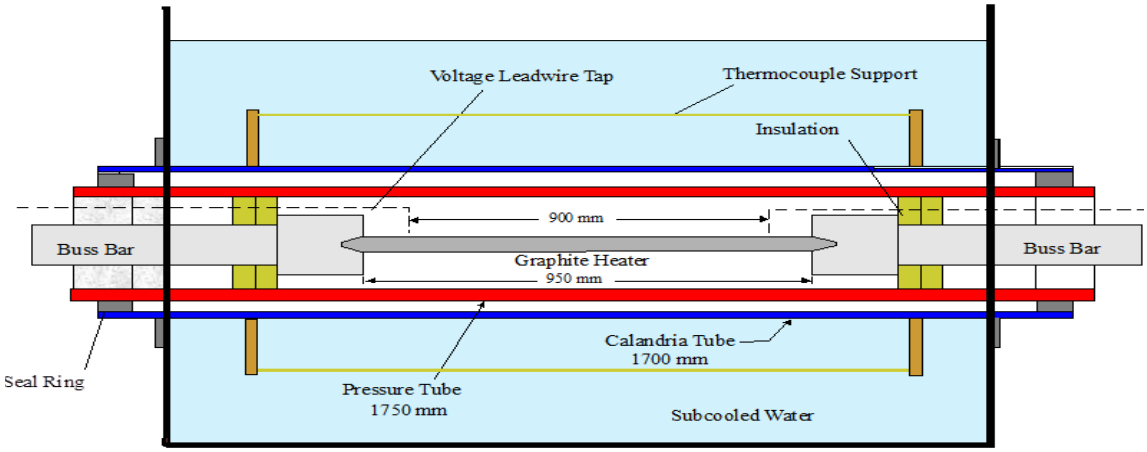

Figure 1 Sketch showing test section and water tank dimensions

The test section is instrumented with over fifty thermocouples, measuring both PT and CT temperatures at various axial and circumferential locations. Four resistance temperature detectors (RTDs) are placed inside the water tank to measure water temperatures around the CT. Direct-current power to the heater is determined from voltage and current measurements. Pressure in the gas (argon) space inside the PT is measured with Rosemount pressure transducers, and is automatically controlled to a desired value with the use of a feed and bleed system. Two video cameras are used to record the entire test through the windows on either side of the water tank.

The test procedure involves bringing the water in the tank to the desired temperature/subcooling, pressurizing the test section to the target pressure, then ramping the power to the heater over about 20 seconds and maintaining it at a constant value as the PT heats, balloons and contacts the CT. The test is terminated about 60 seconds after the contact by switching off power and releasing pressure.

3. Simulation tool

Numerical simulations were performed by implementation of mathematical models in MATLAB R2013a scripts. Details about nodalization, heat transfer models and numerical solvers are presented in the following sections.

3.1 Nodalization

A typical nodalization consists of:

Heater:	5 radial and 30 circumferential nodes
Pressure tube:	40 axial, 3 radial and 36 circumferential nodes
Calandria tube:	40 axial, 2 radial and 36 circumferential nodes

It should be noted that a mesh and time step convergence analysis has been performed and several meshes and time steps were tested. In the current context, "typical nodalization" denotes an average mesh, with an optimized resolution and computation requirements.

3.2 Models of main phenomena

3.2.1 Heat conduction

The general differential equation that describes the heat diffusion with internal heat generation in cylindrical coordinates [5] has the following form:

$$\frac{1}{r}\frac{\partial}{\partial r}\left(r\kappa\frac{\partial T}{\partial r}\right)+\frac{1}{r^2}\frac{\partial}{\partial \phi}\left(\kappa\frac{\partial T}{\partial \phi}\right)+\frac{\partial}{\partial z}\left(\kappa\frac{\partial T}{\partial z}\right)+q_v=\rho c_p\frac{\partial T}{\partial t} \quad (1)$$

In equations (1) T is the temperature, κ, ρ and c_p are thermal conductivity, density and heat capacity of the material. In order to obtain a numerical solution, each equation was discretized using forward difference in time and central difference in space (FTCS) method (see Figure 2). The resulting finite-difference scheme was explicit, first order in time and second-order in spatial variables.

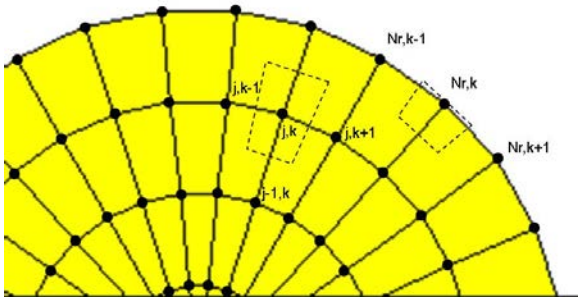

Figure 2 Example of discretization of a cylindrical domain; boundaries of an internal node and an external node are presented

The general discretized form of equation (1), applicable for *internal nodes* has the form:

$$\frac{T_{i,j,k}^{n+1}-T_{i,j,k}^{n}}{\Delta t}=\frac{1}{\rho c_p}\left[\kappa_{i-\frac{1}{2},j,k}\frac{T_{i-1,j,k}^{n}-T_{i,j,k}^{n}}{(\Delta z)^2}-\kappa_{i+\frac{1}{2},j,k}\frac{T_{i,j,k}^{n}-T_{i+1,j,k}^{n}}{(\Delta z)^2}\right]+$$
$$+\frac{1}{\rho c_p}\left[\kappa_{i,j-\frac{1}{2},k}\frac{\left(T_{i,j-1,k}^{n}-T_{i,j,k}^{n}\right)}{(\Delta r)^2}\frac{r_{j-\frac{1}{2}}}{r_j}-\kappa_{i,j+\frac{1}{2},k}\frac{\left(T_{i,j,k}^{n}-T_{i,j+1,k}^{n}\right)}{(\Delta r)^2}\frac{r_{j+\frac{1}{2}}}{r_j}\right]+ \quad (2)$$
$$+\frac{1}{\rho c_p}\left[\kappa_{i,j,k-\frac{1}{2}}\frac{T_{i,j,k-1}^{n}-T_{i,j,k}^{n}}{\left(r_j\Delta\theta\right)^2}-\kappa_{i,j,k+\frac{1}{2}}\frac{T_{i,j,k}^{n}-T_{i,j,k+1}^{n}}{\left(r_j\Delta\theta\right)^2}\right]+\frac{q_v}{\rho c_p}$$

where κ is the thermal conductivity, i, j and k are the node axial, radial and circumferential indices, n is the time step index ρ and c_p are respectively the density and heat capacity of material. Solution of (2) returns the temperature at the next time step ($n+1$) as function of known temperatures at the current time step (n).

For nodes located at the boundary (e.g. at the heater surface or pressure tube surface), the discretized equation was derived based on the first principle, which balances heat transmitted by conduction from the neighboring cells, internal heat generated (q_v) and heat removed by convection and radiation at the boundary (q").

For a node located at an inside boundary that receives a net incident heat flux q", the general discretized equation is:

$$\frac{T_{i,j,k}^{n+1}-T_{i,j,k}^{n}}{\Delta t}=\frac{1}{\rho c_p}\left[\kappa_{i-\frac{1}{2},j,k}\frac{T_{i-1,j,k}^{n}-T_{i,j,k}^{n}}{(\Delta z)^2}-\kappa_{i+\frac{1}{2},j,k}\frac{T_{i,j,k}^{n}-T_{i+1,j,k}^{n}}{(\Delta z)^2}\right]+$$
$$+\frac{1}{\rho c_p}\left[\frac{2q''R_I}{\left(R_I+\frac{\Delta r}{4}\right)\Delta r}-2\kappa_{i,j+\frac{1}{2},k}\frac{T_{i,j,k}-T_{i,j+1,k}}{(\Delta r)^2}\frac{R_I+\frac{\Delta r}{2}}{R_I+\frac{\Delta r}{4}}\right]+ \quad (3)$$
$$+\frac{1}{\rho c_p}\left[\kappa_{i,j,k-\frac{1}{2}}\frac{T_{i,j,k-1}^{n}-T_{i,j,k}^{n}}{R_I\left(R_I+\frac{\Delta r}{4}\right)(\Delta\theta)^2}-\kappa_{i,j,k+\frac{1}{2}}\frac{T_{i,j,k}^{n}-T_{i,j,k+1}^{n}}{R_I\left(R_I+\frac{\Delta r}{4}\right)(\Delta\theta)^2}\right]+\frac{q_v}{\rho c_p}$$

Similarly, for an outside boundary node, which emits net heat flux q", the discretized heat conduction equation has the following form:

$$\frac{T_{i,j,k}^{n+1}-T_{i,j,k}^{n}}{\Delta t}=\frac{1}{\rho c_p}\left[\kappa_{i-\frac{1}{2},j,k}\frac{T_{i-1,j,k}^{n}-T_{i,j,k}^{n}}{(\Delta z)^2}-\kappa_{i+\frac{1}{2},j,k}\frac{T_{i,j,k}^{n}-T_{i+1,j,k}^{n}}{(\Delta z)^2}\right]+$$
$$+\frac{1}{\rho c_p}\left[2\kappa_{i,j-\frac{1}{2},k}\frac{T_{i,j-1,k}-T_{i,j,k}}{(\Delta r)^2}\frac{R_o-\frac{\Delta r}{2}}{R_o-\frac{\Delta r}{4}}-\frac{2q''R_o}{\left(R_o-\frac{\Delta r}{4}\right)\Delta r}\right]+ \quad (4)$$
$$+\frac{1}{\rho c_p}\left[\kappa_{i,j,k-\frac{1}{2}}\frac{T_{i,j,k-1}^{n}-T_{i,j,k}^{n}}{R_0\left(R_0-\frac{\Delta r}{4}\right)(\Delta\theta)^2}-\kappa_{i,j,k+\frac{1}{2}}\frac{T_{i,j,k}^{n}-T_{i,j,k+1}^{n}}{R_0\left(R_0-\frac{\Delta r}{4}\right)(\Delta\theta)^2}\right]+\frac{q_v}{\rho c_p}$$

In equations (3) and (4), R_I and R_o represent the inner and the outer radii of the cylinder, respectively.
Equations (2) to (4) are applied to the heater or the pressure tube, with the following simplifications:

- for the heater, no axial conduction, 2-D (radial and circumferential) approximation;
- for pressure tube and calandria tube, no internal heat generation;

It is worth noting that the application of equation (3) for the central node of the heater may lead to singularities, since R_I=0. In order to address this aspect, the central node of the heater was modeled as a cylinder with uniform temperature and internal heat generation and the radius Δr/2.

3.2.2 Contact conductance

Contact conductance between pressure tube and calandria tube is one of the key parameters of simulation, since it directly controls post-contact heat transfer rate between the pressure tube and calandria tube, and ultimately impacts the boiling regime at the outside of calandria tube. Some experiments to measure the contact conductance directly have been performed [6]. The most reliable estimations of this parameter originate from PT/CT ballooning tests. A relevant study regarding the PT/CT contact conductance, as well as the associated phenomena (PT/CT deformation, heat transfer) is presented in [7]. One important observation is that PT/CT contact conductance is not constant during PT/CT contact transients. More specifically, it is the highest at the time of initial contact and quickly decreases to a steady value, typically much smaller than the initial one. Experimental observations indicate that the higher initial contact conductance, the shorter its duration [1], [7]. The behavior can be explained by the high interfacial pressure at the initial contact, whilst in the post-contact phase, the pressure tube contraction due to cool-down and calandria tube expansion due to heat-up cause the conductance to decrease. Higher initial conductance allows faster expansion/contractions, hence shorter duration of peak conductance. Another observation is that initial contact conductance seems to vary considerably from one geometrical location to another [1]; therefore, it was judged that one single value for a simulation may not be representative. The above observations were included in a conductance model developed in this work, as follows:

1) The contact conductance was assumed to follow a function in time, as presented in Figure 3 and a random distribution in space.
2) An average over the surface value of initial contact conductance was determined. The process involved a few runs with different average values, which were compared with the dryout maps and the dryout times from experiments. From the benchmarked cases, an average contact conductance of 12.7 $kWm^{-2}K^{-1}$ was determined. After the initial PT/CT contact, it was assumed that the contact conductance decreases to 1 $kWm^{-2}K^{-1}$. This value was estimated from the ICSP experimental data.
3) A range of variation of maximum conductance was selected. For the current simulations, a range of ±50% the average value was adopted. That is, the initial contact conductivity ranges from a minimum of 6.3 to maximum of 19.1 $kWm^{-2}K^{-1}$. This range of variation is consistent with observations from previous contact boiling tests.
4) Each finite surface pair pressure tube –calandria tube was randomly allocated a contact conductance selected from the conductivity range defined previously.

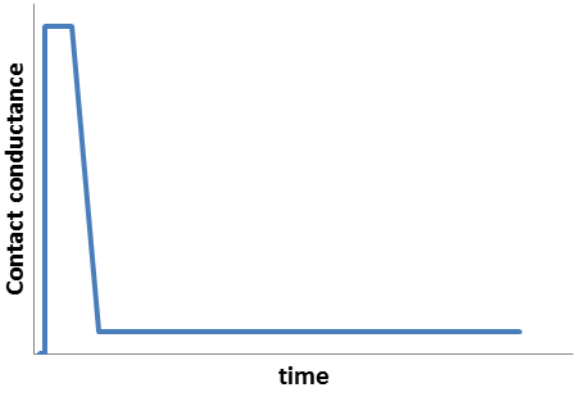

Figure 3 Transient variation of surface averaged PT/CT contact conductance

3.2.3 Free convection and radiation

Table 1A in the Annex summarizes equations and correlations selected to model free convection and radiation between heater and pressure tube, pressure tube and calandria tube and outside of calandria tube.

3.2.4 Pressure tube and calandria tube deformation

Pressure tube/calandria tube deformation was modeled by the methodology presented by Shewfelt [8]. A detailed description is given in Table A2 in the Annex.

Before PC/CT contact, the PT is subject to internal argon pressure, thus only the pressure tube will deform. Hoop stress of pressure tube is:

$$\sigma_{PT} = \frac{P_{Ar} r_{PT}}{\tau_{PT}} \quad (5)$$

After full circumferential contact with CT, both PT and CT interact and an interfacial pressure develops. Interfacial pressure tends to suppress further deformation of pressure tube while simultaneously increasing the hoop stress of calandria tube. Deformation of post contact PTCT was modeled by assuming that that after the initial contact, outside PT and inside CT radii are equal (within a small allowance) at each time step.

Post contact hoop stresses were calculated as:

$$\sigma_{PT} = \frac{(P_{Ar} - P) r_{PT}}{\tau_{PT}} \qquad (6)$$

$$\sigma_{CT} = \frac{P \cdot r_{CT}}{\tau_{CT}}$$

where P_{Ar} denotes internal pressure tube argon gauge pressure, P – PT/CT interfacial pressure, r_{PT}, r_{CT} – average radius of pressure tube and calandria tube respectively, τ_{PT}, τ_{CT} – thickness of pressure tube and calandria tube respectively.

4. Results

4.1 Benchmarking

Code benchmarking was performed against three contact boiling tests, ICSP, CSCB1, and CSCB2. All three tests resulted in plastic deformation of both PT and CT, with measurable CT strain. ICSP and CSCB1 were performed under significantly different conditions, nevertheless both resulted in CT <1%, without PT/CT failure. The test CSCB2 was similar to CSCB1, however it resulted in PT/CT failure (see Table1). For the current benchmarking, the main parameter of interest was the CT hoop strain. In general, the simulation results were relatively close to the experiments. PT/CT contact times, and PT heat-up rates were predicted with very good accuracy. Nevertheless, it was noticed that the PT temperatures at the time of contact and CT temperatures during film boiling were underestimated, typically by 30 to 70K. Shewfelt equations are highly non-linear and relatively sensitive to the temperature. Thus, if PT and CT temperatures are underestimated, it requires significantly longer dryout times to achieve the same strain as in the experiments. In order to address this issue, a correction of 65K was applied to the temperature term in Shewfelt creep strain equation for the calandria tube. It should be noted that other temperatures in the mathematical models (e.g. conduction equations) were not affected by this correction. Also, given the random nature of important phenomena such as the local contact conductance or boiling heat transfer, the benchmarking was based on approximations rather than an exact match.

Numerical simulations have been performed with initial and boundary conditions (such as pressure and the power) from the experiments. Some simulation parameters have been calibrated to reasonably match the predictions. Their description and values used in simulations are provided in the previous Sections and the Annex. A summary of relevant simulations results and comparison with the measured values are presented in Table 1.

Table 1 Non transient and transient benchmarking parameters

	ICSP		CSCB1		CSCB2	
	Exp	Sim	Exp	Sim	Exp	Sim
Moderator subcooling (°C)	29.6	-	24.4	-	23.2	-
PT average heat up rate (350-650°C) (°C/s)	21.8	21.7	15.7	15.6	15.6	15.6
PT top heat up rate (350-650°C) (°C/s)	20	20.2	14.7	14.5	14.5	14.5
PT middle heat up rate (350-650°C) (°C/s)	21.4	21.3	15.3	15.4	15.3	15.4
PT bottom heat up rate (350-650°C) (°C/s)	24.1	23.9	16.9	16.9	16.9	16.9
Time of first PT/CT contact (s)	72	71.4	90	90.3	90	90.3
PT temperature at time of contact, axial centre, 0° (°C)	857.6	813.5	846.6	778	800.5	777
PT temperature at time of contact, axial centre, 90° (°C)	814	799	740	757	747.3	756
PT temperature at time of contact, axial centre, 180° (°C)	863.3	831.7	833	773	809	771
PT true strain at 0° (%)	15.7	16	27.4	25.1	95.3	36
PT true strain at 90°(%)	10.6	11.1	10.5	11.1	14	11.2
PT true strain at 180°(%)	25.5	25.6	25.5	16.9	28.8	17
Time in dryout (s)	21	32	33	43	49	67
CT hoop strain (%)	0.4	0.25	0.35	0.36	9.6	6.41

Examination of values from Table 1 reveals that the model has been able to capture the main phenomena with acceptable accuracy. It should be noted that the large difference between PT true strain at the top in the test CSCB2 (95% vs 36%) can be attributed to the PT/CT rupture, where PT/CT deformation is significantly higher, thus it is expected that Shewfelt creep equation will not hold. In numerical simulations the Shewfelt creep equation were assumed for the whole duration of the transient. In order to enhance our understanding on the effects of the moderator subcooling and pressure heat-up rates on the calandria tube hoop strain, two sensitivity studies have been completed.

4.2 Sensitivity of CT hoop strain to moderator subcooling at constant heat-up rate

For this case, the heat up rate was maintained constant at 15.7 C/s and the moderator subcooling was varied between 26 to 23.2 °C. The simulations show that the sensitivity of CT strain to the moderator subcooling in very low strain range is low (see Figure 4). However, as the CT strain increases, the sensitivity increases significantly. This behaviour can be attributed to the highly non-linear nature of Shewfelt creep equations. The main variables that control creep rate of CT are the temperature, the hoop stress and the time. Experiments and simulations suggest that if the

moderator subcooling decreases, the extent and duration of dryout increase; it also cause higher CT temperatures. The combination of these effects results in a significant increase of CT creep deformation. The predicted behavior is also consistent with the experimental observations from the CSCB1 and CSCB2. Both tests have practically the same PT heat-up rates (15.6 and 15.7 °C/s) but the moderator subcooling of CSCB2 was 1.2 °C lower. The CT hoop strain was much larger for CSCB2, which caused the PT/CT rupture.

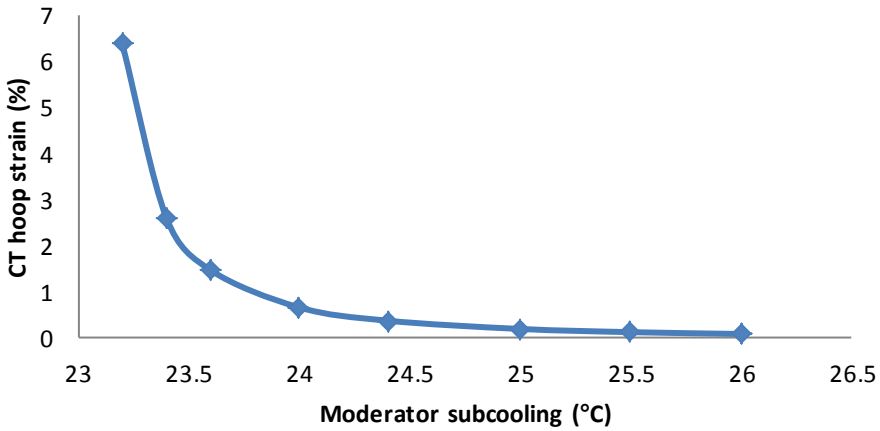

Figure 4 Sensitivity of CT hoop strain to the moderator subcooling at constant PT heat-up rate

4.3 Sensitivity of CT hoop strain to heat up rate at constant moderator subcooling

A complementary analysis at various heat-up rates and constant moderator subcooling, 24.4 °C has been performed and the results are plotted in Figure 5.

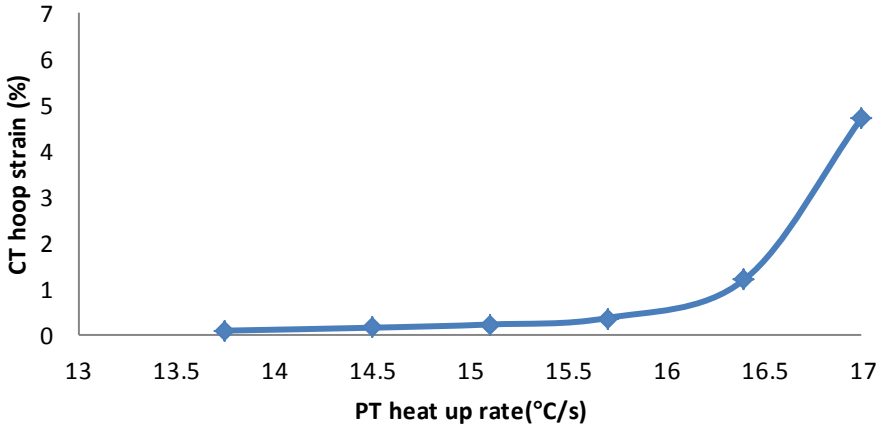

Figure 5 Sensitivity of CT hoop strain to PT heat-up rate the at constant moderator subcooling

The CT strain shows non-linear behavior above certain heat-up rates. For the selected subcooling, the CT hoop strain increases significantly at heat up rates larger than 16 °C/s.

5. Conclusions

Simulation of contact boiling experiments is very complex, comprising modelling and interaction between thermal and mechanical phenomena and characterized by highly non-linear constitutive equations. Moreover, simulation of experiments where calandria tube undergoes significant deformation brings in supplementary challenges on accurate mathematical representation of PT/CT geometry, hence adequate computation of local hoop stresses.

The random nature and relatively large uncertainties of some important simulation phenomena, such as PT/CT thermal contact conductance or heat transfer coefficient during various boiling regimes, contribute to the relatively large simulation uncertainties. In this context, the sensitivity of creep rate equations to temperature implies that the uncertainties in predicted PT and CT temperatures may cause relatively large uncertainties of the predicted strain of the calandria tube. That is, in order to obtain acceptable CT strains, the predicted temperatures, hoop stresses and time of dryout must have relatively narrow uncertainty ranges.

It appears that CT hoop strain shows non-linear behaviours (i.e. cliff-edge effects) both versus moderator subcooling and heat up rate, at plastic strain larger than 1%. This need to be further investigated at various moderators subcoolings and PT heat-up rates.

It seems that CT can sustain 2% plastic strain without failure, if the straining is arrested by timely rewet. The results of sensitivity studies suggest that the conditions leading to 2% CT strain may be too close to channel failure conditions and too close to the region of cliff edge effects, thus it is prudent that these regimes be avoided in accident analysis.

The applicability and overall accuracy of mathematical models and simulation parameters need to be improved further by benchmarking against more experiments from the CSCB series. As such, the development of a “bulge/bubble deformation model”, better understanding of heat transfer by free convection inside the PT, circumferential distribution of CHF and axial non uniformities have been identified as possible areas of improvement.

6. References

[1] Oh, D.J. and Lei, Q.M., “Validation of New Moderator Subcooling Methodology”, COG 09-2059, 2010

[2] COG-07-2003, “The State-of-the-Art Report on Fuel Channel Integrity During High-Temperature Transient Events”, December 2009, E-doc #3490316.

[3] El-Hawari,M et al., New Contact Boiling Experiments to Evaluate Calandria Tube Strain Acceptance Criteria, 35th Annual Conference of the Canadian Nuclear Society, May 31-June 03, 2015

[4] Choi, J, Nitheanandan, T., "IAEA ICSP on HWR Moderator Subcooling Requirements to Demonstrate Backup Heat Sink Capabilities of Moderator During Accidents," 34th Annual CNS Conference, Toronto, ON, June 9-12, 2013

[5] Incropera, F. and de Witt, F., "Fundamentals of Heat and Mass Transfer", 6th Edition., John Wiley et Sons Inc., 2006

[6] Shoukri,M and Chan, A.M.C., "On the Thermal Analysis of Pressure Tube/Calandria Tube Contact in CANDU Reactors, Nuclear Engineering and Design, Vol. 104, pp 197-206, 1987

[7] Cziracky, A, "Pressure tube-calandria tube thermal contact conductance – Master Thesis", McMaster University, 2006

[8] Shewfelt, R.S.W et al.,"A High-Temperature Creep Model for Zr-2.5 wt% Nb Pressure Tubes", Journal of Nuclear Materials, Vol. 125, pp 228-235, 1984

[9] Lis. J, Experimental Investigation of Natural Convection Heat Transfer in simple and obstructed annuli, Proceedings of the 3rd International Heat Transfer Conference, Vol.2, pp. 196-204, 1966

[10] Churchill, S.W., and Chu, H.H.S. Int. J. Heat Mass Transfer, 18, 1049, 1975

[11] Leung, L.H.K. and Groeneveld, D. (Editors), "Compendium of Thermalhydraulics Correlations and Fluid properties," version 1991, Rev 2, ARD-TD-243

[12] Thibault, J. "Boiling Heat Transfer Around a Horizontal Cylinder and in Tube Bundles, PhD Thesis", McMaster University, 1978

[13] Bjornard, T.A. and Griffith, P., "PWR Blowdown Heat Transfer", Proceedings ASME Symposium on the Thermal and Hydraulic Aspects of Nuclear Reactor Safety, Vol. 1, p 17-41, Atlanta, Georgia, 1997

[14] Gillespie, G. and Moyer, R. "An Experimental Determination of Heat Transfer from Large Cylinders: Film Boiling in Subcooled Water", WNRE-569, Atomic Energy of Canada Limited, 1984

ANNEX

Table A1 Correlations for convection and radiation heat transfer

Location	Phenomenon	Equation	Observations
Graphite heater - pressure tube	Free convection	Lis (1966) [9]: $\frac{k_{eff}}{k} = 0.389\left[Ra_{Di}\left(1-\frac{Di}{D_o}\right)\right]^{0.237}$ $\frac{k_{eff}}{k} = 0.087\left[Ra_{Di}\left(1-\frac{Di}{D_o}\right)\right]^{0.329}$	$4\cdot10^4 < Ra_{Di}\left(1-\frac{D_i}{D_o}\right)^{6.5} < 1\cdot10^8$ $1\cdot10^8 < Ra_{Di}\left(1-\frac{D_i}{D_o}\right)^{6.5} < 1\cdot10^{10}$
	Thermal radiation	$q_{rad} = \frac{\sigma(T_1^4 - T_2^4)}{\frac{1-\varepsilon_1}{A_1\varepsilon_1} + \frac{1}{A_1F_{12}} + \frac{1-\varepsilon_2}{A_2\varepsilon_2}}$ $F_{i\to j} = \frac{1}{A_i}\int_{A_i}\int_{A_j}\frac{\cos\theta_i\cos\theta_j}{\pi r^2}dA_i dA_j$ $F_{i\to j} = \frac{1}{A_i}\sum_i\sum_j\frac{\cos\theta_i\cos\theta_j}{\pi r_{i\to j}^2}\Delta A_i\Delta A_j$	*1) Initial (un-deformed) geometry* This view factor matrix was applied from the start of the simulation until central axial ring of the pressure tube crept by 1%. *2) Intermediate deformation* The pressure tube radius is calculated as the average of initial value and the value at the contact with the calandria tube. This matrix was selected when deformation of central axial ring exceeded 1% until pressure tube/calandria tube contact occurred. *3) Post deformation* Final view factor matrix assumed the pressure tube radius at the contact with calandria tube, and which was maintained until the end of the simulation. It should be noted that if after the contact pressure tube/calandria tube undergoes significant deformation (which was not the case for the current simulation) the view factor matrix require subsequent updates.
Outer surface pressure tube -	Free convection	$q = \frac{2\pi L_h k_{eff}(T_i - T_0)}{\ln(r_0/r_i)}$	k_{eff} was assumed equal to molecular thermal conductivity of annulus gas, CO_2

inner surface calandria tube (annulus)	Thermal radiation	$q_{rad} = \frac{\sigma(T_1^4 - T_2^4)}{\frac{1-\varepsilon_1}{A_1\varepsilon_1} + \frac{1}{A_1 F_{12}} + \frac{1-\varepsilon_2}{A_2\varepsilon_2}}$	The analysis assumes that F_{12} is unity, that is, all thermal radiation that leaves an elementary surface of PT is intercepted by the homologous surface of the CT
Outer surface calandria tube	Single phase free convection	Churchill and Chu (1968) [10]: $Nu_D = \left\{0.6 + \frac{0.387 Ra_D^{1/6}}{\left[1 + (0.559/\mathrm{Pr})^{9/16}\right]^{8/27}}\right\}^2$	
	Nucleate boiling	Forster and Zuber (1955) [11]: $q'' = 0.00122\left(\frac{k_f^{0.79} c_{pf}^{0.45} \rho_f^{0.49}}{\sigma^{0.5} \mu_f^{0.29} h_{fg}^{0.24} \rho_g^{0.24}}\right)\left[T_w - T_{sat}(P_f)\right]^{1.24} \Delta P_{sat}^{0.75}$	
	Critical heat flux	Zuber correlation of Lienhard [11]: $q_{CHFsat} = 0.118 h_{fg}\left[\sigma g \rho_g^2 (\rho_f - \rho_g)\right]^{0.25}$ For subcooled CHF, Thibault (1978) [12]: $q_{CHF} = q_{CHFsat}\left[1 + 0.0437(T_{sat} - T_0)\right]$	
	Transition boiling	Bjonard and Griffith [13]: $q_{TB} = \lambda q_{CHF} + (1-\lambda) q_{mfb}$ $\lambda = \left[\frac{(T_{mfb} - T_W)}{(T_{mfb} - T_{CHF})}\right]^2$	
	Rewetting temperature	$T_{rew} = 2.38\Delta T_{sub} + 446.3$ $T_{rew} = 5.86\Delta T_{sub} + 341.9$	ΔT_{sub}<30 K ΔT_{sub}>30 K
	Film boiling	Gillespie-Moyer [14]: $h_{fb} = h_{fb0}\left[1 + 0.031(T_{sat} - T_l)\right]$ h_{fb0}=200 $Wm^{-2}K^{-1}$.	

Table A2 PT/CT creep deformation

Conditions	Equation	Observations
PT/CT temperatures between 450 to 850°C	$\dot{\varepsilon} = 1.3 \cdot 10^{-5} \sigma^{9} \exp\left(-\frac{36600}{T}\right) + \frac{5.7 \cdot 10^{7} \sigma^{1.8} \exp\left(-\frac{29200}{T}\right)}{\left[1 + 2 \cdot 10^{10} \int_{t_1}^{t} \exp\left(-\frac{29200}{T}\right) dt\right]^{0.42}}$	$\dot{\varepsilon}$ - pressure tube creep rate, T – absolute temperature (K) σ – hoop stress (MPa), t_1 – time when T=973K and t_2 – time when T=1123K.
PT/CT temperatures between 850 and 1200°C	$\dot{\varepsilon} = 10.4 \sigma^{3.3} \exp\left(-\frac{19600}{T}\right) + \frac{3.5 \cdot 10^{10} \sigma^{1.4} \exp\left(-\frac{19600}{T}\right)}{1 + 274 \int_{t_2}^{t} \exp\left(-\frac{29200}{T}\right) (T - 1105)^{3.72} dt}$	